condensed matter

MDPI

Article

MgB_2 Thin Films Fabricated by Pulsed Laser Deposition Using Nd:YAG Laser in an In Situ Two-Step Process

Toshinori Ozaki [1,*], Satoshi Kikukawa [1], Rika Tanaka [2], Akiyasu Yamamoto [2], Akihiro Tsuruta [3] and Yuji Tsuchiya [4]

[1] School of Engineering, Kwansei Gakuin University, 1 Gakuen Uegahara, Sanda 669-1330, Japan; iamkikukawa@gmail.com
[2] Department of Applied Physics, Tokyo University of Agriculture and Technology, Koganei 184-8588, Japan; s206525u@st.go.tuat.ac.jp (R.T.); akiyasu@cc.tuat.ac.jp (A.Y.)
[3] National Institute of Advanced Industrial Science and Technology (AIST), Shimosidami, Moriyama-ku, Nagoya 463-8560, Japan; a.tsuruta@aist.go.jp
[4] Institute for Materials Research, Tohoku University, 2-1-1 Katahira, Sendai 980-8577, Japan; tsuchiya@tohoku.ac.jp
* Correspondence: tozaki@kwansei.ac.jp

Abstract: Magnesium diboride (MgB_2) thin films on *r*-cut sapphire (*r*-Al_2O_3) single crystals were fabricated by a precursor, which was obtained at room temperature via a pulsed laser deposition (PLD) method using a Nd:YAG laser, and an in situ postannealing process. The onset superconducting transition, T_c^{onset}, and zero-resistivity transition, T_c^{zero}, were observed at 33.6 and 31.7 K, respectively, in the MgB_2 thin films prepared by a Mg-rich target with a ratio of Mg:B = 3:2. The critical current density, J_c, calculated from magnetization measurements reached up to 0.9×10^6 A cm^{-2} at 20 K and 0 T. The broad angular J_c peak was found at 28 K when the magnetic fields were applied in a direction parallel to the film surface ($\theta = 90°$). This could be indicative of the granular structure with randomly oriented grains. Our results demonstrate that this process is a promising candidate for the fabrication of MgB_2 superconducting devices.

Keywords: superconductor; thin film; critical temperature; critical current

Citation: Ozaki, T.; Kikukawa, S.; Tanaka, R.; Yamamoto, A.; Tsuruta, A.; Tsuchiya, Y. MgB_2 Thin Films Fabricated by Pulsed Laser Deposition Using Nd:YAG Laser in an In Situ Two-Step Process. *Condens. Matter* **2022**, *7*, 48. https://doi.org/10.3390/condmat7030048

Academic Editor: Andrea Perali

Received: 14 June 2022
Accepted: 27 July 2022
Published: 2 August 2022

1. Introduction

Magnesium diboride (MgB_2) with the superconducting transition temperature T_c = 39 K [1] has a great potential for superconducting electronic applications cooled with liquid hydrogen (LH_2) alternative to liquid-helium-based cryogenic systems. In addition to its relatively high T_c, MgB_2 exhibits a lot of fascinating properties, such as a simple layer structure [1], lower anisotropy [2], and longer coherence length [3], when compared with cuprate high-T_c superconductors. Additionally, the transparency of the grain boundaries to current flow [4,5] and the abundance of Mg and B offer the possibility of employing MgB_2 for device applications. Epitaxial MgB_2 films enable the fabrication of the superconducting electronic applications, such as superconducting detectors (transition edge sensors (TES) and superconducting tunnel junctions (STJ)), digital circuits, and diodes [6]. Tremendous progress has been made upon the successful application of a variety of deposition techniques, such as molecular beam epitaxy (MBE) [7], pulsed laser deposition (PLD) [8–15], electron beam evaporation (EBE) [16–18], hybrid physical–chemical vapor deposition (HPCVD) [19–21], reactive evaporation [22], and magnetron sputtering [23]. Two of the most important requirements for the fabrication of MgB_2 thin films are: (*i*) to provide a sufficiently high Mg vapor pressure for phase stability of MgB_2 and (*ii*) to eliminate the residual oxygen during the thin film synthesis because of the high sensitivity of Mg to oxidation. MgB_2 films have been fabricated via the PLD technique soon after the discovery of superconductivity in this material [8–11]. The typical fabrication

process of MgB_2 thin films consists of a precursor, grown by the PLD method at room temperature, and a postannealing process. The postannealing processes are classified as: (*i*) ex situ, which is performed in a metal tube under a Mg atmosphere after the precursor deposition in a chamber [8,9], and (*ii*) in situ, which is performed in the same chamber as the deposition chamber for the precursor films under vacuum, Ar or $Ar/4\%H_2$ atmosphere [10–14]. The MgB_2 films fabricated with a precursor, grown by the PLD method, and in situ postannealed (in situ PLD process) exhibited a zero-field T_c^{zero} of 29 K and a self-field J_c of 2×10^5 A cm^{-2} at 5 K [12].

KrF (λ = 248 nm) excimer lasers are widely used for PLD due to their high photon energy and light intensity. However, these excimer lasers are costly and use poisonous halogen gases for excitation. A feasible way to overcome these drawbacks would be to use a Nd:YAG (neodymium-doped yttrium aluminium garnet; $Nd:Y_3Al_5O_{12}$) solid state laser instead. The Nd:YAG laser is highly stable and safe compared with excimer lasers, which use toxic gas. The fundamental wavelength of the Nd:YAG laser is 1064 nm. However, ultraviolet light can be generated by changing harmonic crystals to the fourth harmonic of the Nd:YAG's fundamental wavelength (λ = 266 nm). At this wavelength, the Nd:YAG laser has a photon energy comparable to the KrF excimer laser's fundamental mode (λ = 248 nm). The Nd:YAG laser also has additional advantages over the excimer lasers associated with their low installation, maintenance costs, and compact footprint. Hence, the Nd:YAG laser could be a potential alternative to excimer lasers for the PLD system. However, there are only few reports on MgB_2 films fabricated by the Nd:YAG laser [14]. In this paper, we report the fabrication of superconducting MgB_2 thin films via an in situ PLD process using the fourth harmonic of the Nd:YAG laser. The influence of the Mg–B target composition on T_c of the films is investigated. We also present the structural and superconducting properties of the obtained MgB_2 films.

2. Materials and Methods

The MgB_2 films were fabricated by a precursor and an in situ postannealing process. The Mg–B precursor films were obtained via the PLD method using the fourth harmonic of a Nd:YAG solid-state laser (Lotis TII, LS2147, Minsk, Belarus). To compensate for a possible loss of Mg due to the high Mg volatility, we prepared Mg-enriched targets with a nominal composition of Mg:B = 2:2, 3:2, and 4:2. These targets were prepared using a spark plasma sintering technique with a fine mixture of metal Mg and laboratory-made MgB_2 powder, synthesized from Mg and B using a modified powder-in-closed-tube technique [24–26], and providing for a highly dense Mg–B target (~100% density) with minimal oxygen incorporation. The ultra-high vacuum (UHV) chamber was evacuated to a base pressure of $\sim 5 \times 10^{-7}$ Pa and subsequently filled with Ar buffer gas (99.9999% purity) purified with gas filters for the removal of remanent O_2 and H_2O molecules in the Ar gas cylinder, to the pressure of ~5 Pa. The precursor layers were amorphous Mg–B film, deposited on *r*-cut sapphire (*r*-Al_2O_3) $(1\bar{1}02)$ single crystals at room temperature for 120 min at a pulse frequency of 10 Hz. After the deposition, these films were postannealed in the same UHV chamber at 780–800 °C for 15 min in an atmosphere of ~0.9 atom purified Ar gas, followed by cooling down to room temperature. The film thickness was typically estimated to be ~200 nm after the postannealing.

The structure of the films was evaluated by grazing incidence X-ray diffraction (GIXRD) in SmartLab (Rigaku) with Cu-Kα radiation. The GIXRD scan was collected with a grazing incidence angle of 0.5°. The magnetization, *M*, was measured via a superconducting quantum interference device (SQUID, Quantum Design) magnetometer with a perpendicular applied field *H* to the film surface. The critical temperature, T_c^{mag}, was determined as the bifurcation of zero-field cooling (ZFC) and field cooling (FC) in $M(T)$ curves. Electrical transport measurements were carried out with a standard four-probe method in a physical property measurement system (PPMS and DynaCool, Quantum Design). A 100 μm wide by 1 mm long bridge was fabricated by laser cutting for transport measurements. The film was mounted on a rotator holder in the maximum Lorentz force

configuration, where the current direction is always perpendicular to the applied magnetic field, and the film was rotated around this current axis. In this paper, we define the direction of the applied magnetic fields $\theta = 0^\circ$ and 90° as the magnetic fields perpendicular and parallel to the film surface, respectively. The critical current density J_c was determined from *I*–*V* curves using a 1 μV cm^{-1} criterion. T_c^{onset} was defined as the temperature where resistivity starts to deviate from the extrapolated normal-state behavior, while T_c^{zero} was defined as a resistivity criterion of 0.1 μΩ cm.

3. Results and Discussion

Figure 1 shows the temperature dependences of magnetization for the three films fabricated using target pellets with a nominal composition of Mg:B = 2:2, 3:2, and 4:2 with an $H \perp$ film surface. The measurements were performed under 10 Oe to evaluate the shielding and Meissner regions, corresponding to ZFC and FC curves, respectively. T_c^{mag} values were estimated to be 29.0, 31.2, and 15.5 K for the films fabricated with the target ratio of Mg:B = 2:2 (film #1), 3:2 (film #2), and 4:2 (film #3), respectively. Film #3 shows the lowest T_c^{mag} of 15.5 K among the three films with a very small diamagnetic shielding signal in the ZFC curve, which is nearly overlapped with FC curves for films #1 and #2. The reason for the observed lower T_c^{mag} is considered to be that the film composition deviates from the stoichiometry. The small diamagnetic signal of film #3 also indicates that the superconducting phase would be present in a filamentary-like manner because of excess Mg. Film #2 with the highest T_c^{mag} of 31.2 K shows a very steep transition under zero-field-cooling (ZFC) condition with large shielding fraction. On the other hand, diamagnetic signal in the FC process is very small, which arises from strong vortex pinning in the film. The temperature dependence of the electrical resistivity of film #2 at 0 T is shown in Figure 2. The inset is a magnified view around the T_c region. A sharp transition is evident in Figure 2. The onset- and zero-resistivity temperatures were estimated to be T_c^{onset} = 33.6 K and T_c^{zero} = 31.7 K, respectively. The residual resistivity ratio (RRR = ρ(300 K)/ρ(40 K)) was calculated to be 1.3, which is consistent with previous reports [11,12,15]. The low RRR value would be ascribed to fine structure [12] and/or phase purity [19] and/or less amount of unreacted Mg [27]. The T_c value of film #2 is shown to be higher than those observed in previous PLD-fabricated MgB_2 films via in situ and ex situ processes using a Nd:YAG laser [14] or the in situ process utilizing an excimer laser [10–13]. This could be attributed to the use of a highly dense Mg–B target and a high vacuum background pressure of ~5 × 10^{-7} Pa in this study. However, the obtained T_c value is still lower than the original T_c of MgB_2 [1] and MgB_2 films fabricated by other processes [7–9,15–21] including the ex situ process with the excimer laser [8,9].

In order to analyze the crystal structure of the film, the GIXRD measurement, which can avoid intense signal from the substrate and obtain stronger signal from the film, was performed. Figure 3 displays the GIXRD patterns for MgB_2 film #2. The relative peak intensity in the GIXRD measurement could be indicative of the presence of the MgO phase other than the MgB_2 phase. The occurrence of the MgO phase would result from little amount of residual oxygen in the Mg–B target and supplied Ar gas. The absence of MgB_2 peaks may be attributed to poor crystallinity [28].

Figure 4a presents the magnetic field dependence of J_c for MgB_2 film #2 at 5, 10, and 20 K with the magnetic field applied perpendicular to the film surface. J_c was calculated from the magnetization hysteresis (*M*-*H*) loops using Bean's critical-state model [29,30]. For rectangular prism-shaped superconductors of dimensions $a < b$, the in-plane critical current density J_c^{ab} for an $H \perp$ film surface is given by $J_c^{ab} = 20\Delta M/(a(1 - a/3b))$, where ΔM is the difference in magnetization, M (emu cm^{-3}), between the upper and lower branches of the *M*-*H* loop. In the inset of Figure 4a, the *M*-*H* loop in film #2 is plotted. At 5 K, the $M(H)$ in low magnetic fields has an irregular shape, which is characteristic of a flux jump, whereas the $M(H)$ in high magnetic fields varies smoothly with increasing and decreasing magnetic fields. The presence of flux jumps was observed just after the discovery of superconductivity in MgB_2 material [31,32]. The J_c(0 T) values were obtained

to be 1.9 × 10^6 and 0.9 × 10^6 A cm^{-2} for 10 and 20 K, respectively. The J_c values were decreased rapidly with increasing applied magnetic fields. The transport J_c as a function of magnetic fields up to 1 T ⊥ film surface for MgB_2 film #2 at different temperatures is shown in Figure 4b. The transport J_c(1 T) at 20 K is about one-third of the value of one of the MgB_2 wires [33].

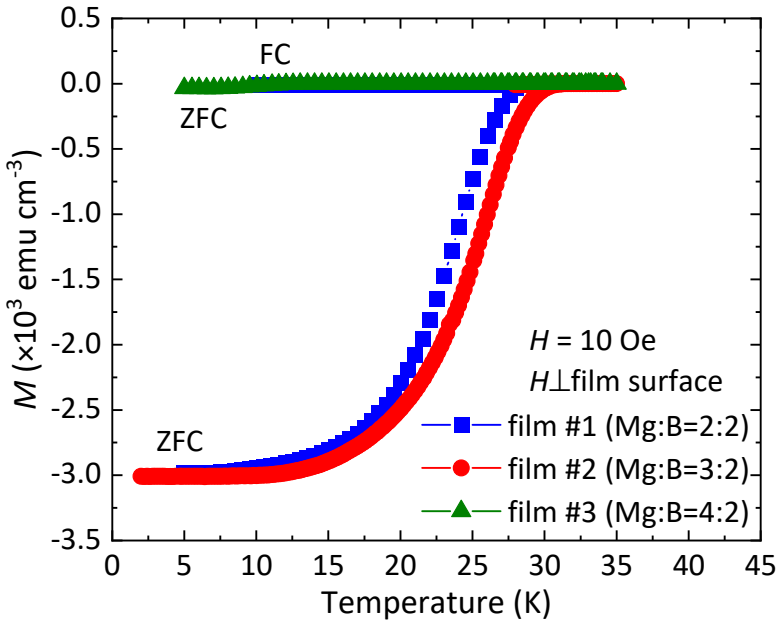

Figure 1. Temperature dependence of magnetization *M* for both zero-field-cooling (ZFC) and field-cooling (FC) processes at a magnetic field of *H* = 10 Oe applied in the direction perpendicular to the film surface for the three films (films #1, #2, and #3) fabricated using three target pellets with a nominal composition of Mg:B = 2:2 (film #1), 3:2 (film #2), and 4:2 (film #3), respectively.

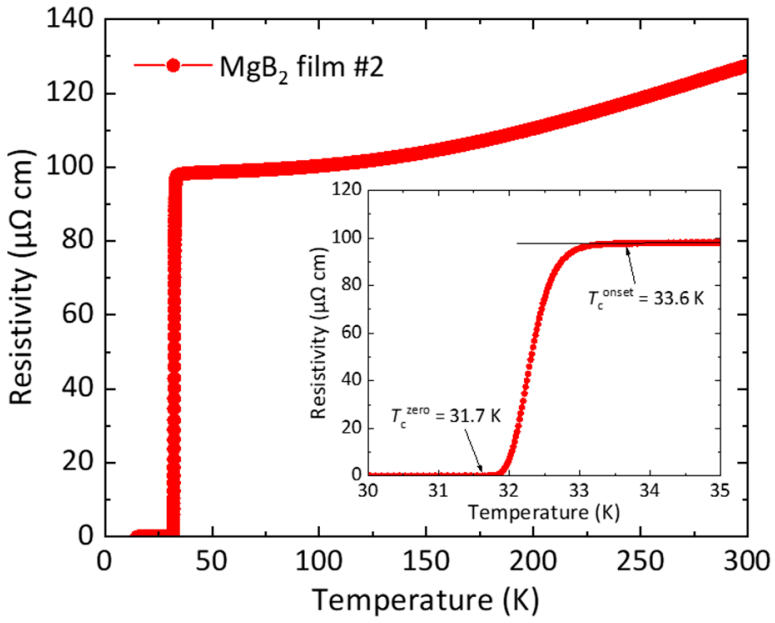

Figure 2. Temperature dependence of the electrical resistivity for the MgB_2 film prepared by the Mg:B = 3:2 target (film #2). The inset enlarges the resistivity curve around the superconducting transition.

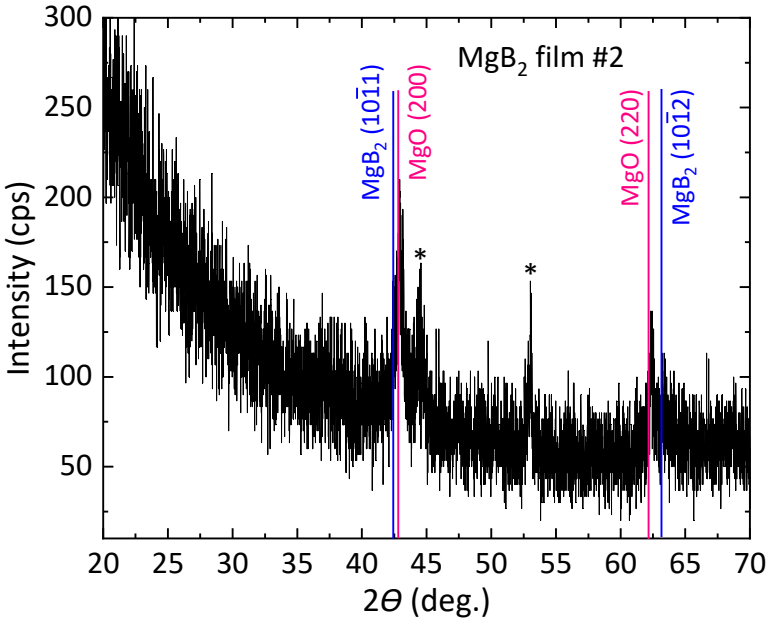

Figure 3. The grazing incidence x-ray diffraction (GIXRD) patterns at an incidence angle of 0.5° for the MgB_2 film prepared by the Mg:B = 3:2 target (film #2). Minor peaks marked by asterisks, *, correspond to additional minor phases.

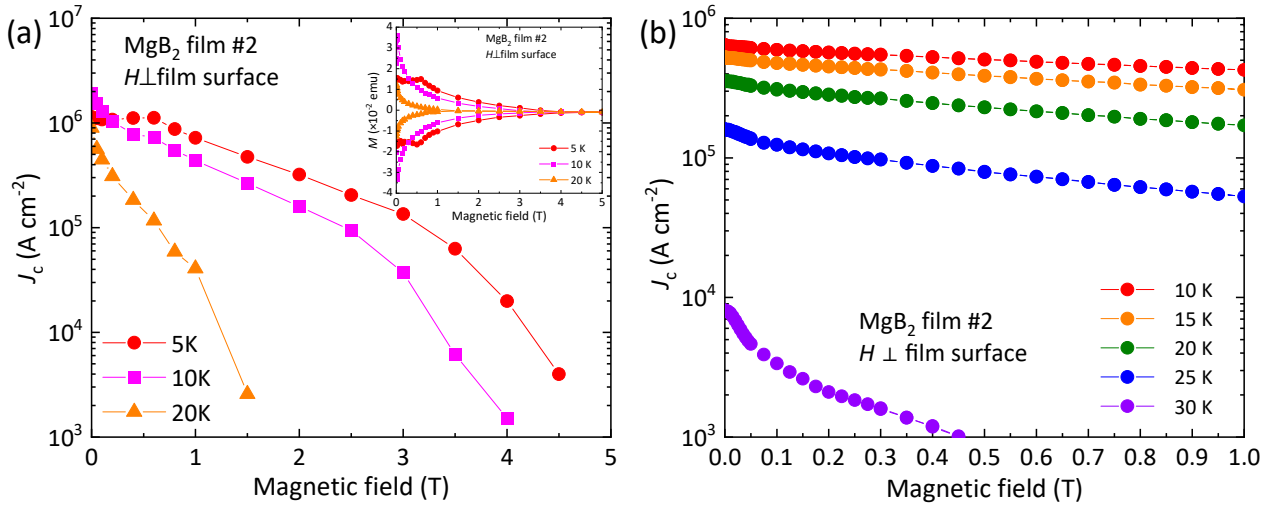

Figure 4. (**a**) Magnetic field dependence of the critical current density J_c at 5, 10, and 20 K calculated using Bean's critical-state model [29,30] for the MgB_2 film prepared by Mg:B = 3:2 target (film #2). The magnetic field is applied perpendicular to the film surface. The inset shows a magnetic hysteresis loop under an $H \perp$ film surface. (**b**) Magnetic field dependence of the transport critical current density J_c at different temperatures up to 1 T for the MgB_2 film prepared by the Mg:B = 3:2 target (film #2). The magnetic field is applied perpendicular to the film surface.

Figure 5 shows the angular dependence of transport J_c for MgB_2 film #2 at 28 K up to 0.8 T. J_c exhibits a broad maximum at $\theta = 90°$ (H // film surface) and no prominent J_c peak at $\theta = 0°$ ($H \perp$ film surface). J_c-anisotropy values, γ_{Jc} ($J_c^{90°}/J_c^{0°}$), of 2.0, 2.6, and 2.0 were observed at 0.03, 0.1, and 0.3 T, respectively, indicating that the applied magnetic fields have only a small impact on γ_{Jc} in this measurement condition. Seminal works by Kitaguchi et al. showed that the MgB_2 films on *c*-cut sapphire (*c*-Al_2O_3) (0001) single crystals fabricated by EBE technique have two pinning mechanisms [16]. One would be attributed to grain boundaries pinning originating in the columnar grain microstructure, leading to the strong

peak around an $H \perp$ film surface. The other would be caused by the film surface, the MgB_2/substrate interface, or the layer structure of the crystals, leading to the strong peak around an H // film surface. The MgB_2 film on c-cut sapphire (c-Al_2O_3) single crystals fabricated by an ex situ PLD process has a broad and small peak at an H // film surface [34]. This could be because of the granular structure with randomly oriented grains in the films. MgB_2 film #2 on r-Al_2O_3 single crystals in this study has also a broad peak at an H // film surface. These results indicate that the broad peak would arise from the granular grain structure. In addition, we found that the difference of the crystallographic orientation on an Al_2O_3 substrate would contribute little to the peak position in $J_c(\theta)$ curves for MgB_2 films in this measurement.

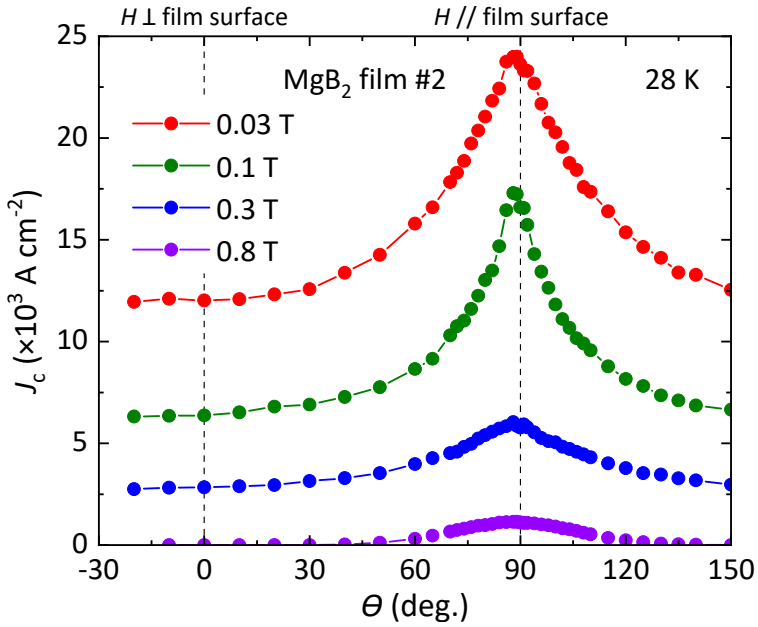

Figure 5. Angular field dependence of the critical current density J_c obtained from transport measurement at 28 K up to 0.8 T for the MgB_2 film prepared by the Mg:B = 3:2 target (film #2).

4. Conclusions

Superconducting MgB_2 thin films were prepared via an in situ PLD process using the fourth harmonic of the Nd:YAG laser. MgB_2 film #2 prepared with a nominal composition of Mg:B = 3:2 shows a superconducting transition at T_c^{zero} of 31.7 K and T_c^{mag} of 31.2 K. The obtained T_c is one of the highest in the MgB_2 films prepared by the PLD process using the Nd:YAG laser. Magnetic hysteresis measurements show that J_c^{ab}(0 T) of MgB_2 film #2 is estimated to be $\sim 0.9 \times 10^6$ A cm^{-2} at 20 K. The transport measurement in the angular dependence of J_c in the magnetic field demonstrates that MgB_2 film #2 has higher J_c at $\theta = 90^\circ$ (H // film surface), which could reflect the granular grain structure. We expect to achieve higher superconducting properties by fine tuning of the fabrication process. Our results indicate that the in situ preparation procedure with Nd:YAG laser processes would be favorable for the fabrication of superconducting devices over the excimer laser process.

Author Contributions: Conceptualization, T.O.; sample preparation, R.T., A.Y., S.K. and T.O.; transport measurement, S.K., Y.T. and T.O.; magnetization measurement, S.K. and T.O.; GIXRD measurements, S.K.; data curation, S.K., Y.T. and T.O.; writing—original draft preparation, T.O.; writing—review and editing, A.Y., A.T. and Y.T. All authors have read and agreed to the published version of the manuscript.

Funding: This work was supported by the New Energy and Industrial Technology Development Organization (NEDO). It was also supported by a Grant-in-Aid for Scientific Research from the Japan Society for the Promotion of Science under grant nos. 20K15217, 21H01615, and 22H01522.

Institutional Review Board Statement: Not applicable.

Informed Consent Statement: Not applicable.

Data Availability Statement: Datasets acquired during the present research are available from the corresponding author on reasonable request.

Acknowledgments: The authors appreciate Y. Yoshida (Nagoya University) for the support in the transport measurement with a PPMS. The authors also appreciate M. Fukuzumi (Hyogo Prefectural Institute of Technology) for the technical assistance in the GIXRD measurement. We thank Dimitrov I. K. for the critical reading of the manuscript.

Conflicts of Interest: The authors declare no conflict of interest.

References

1. Nagamatsu, J.; Nakagawa, N.; Zenitani, Y.; Akimitsu, J. Superconductivity at 39 K in magnesium diboride. *Nature* **2001**, *410*, 63–64. [CrossRef]
2. Fletcher, J.D.; Carrington, A.; Taylor, O.J.; Kazakov, S.M.; Karpinski, J. Temperature-dependent anisotropy of the penetration depth and coherence length of MgB_2. *Phys. Rev. Lett.* **2005**, *95*, 097005. [CrossRef] [PubMed]
3. Buzea, C.; Yamashita, T. Review of the superconducting properties of MgB_2. *Supercond. Sci. Technol.* **2001**, *14*, R115–R146. [CrossRef]
4. Bugoslavsky, Y.; Perkins, G.K.; Qi, X.; Cohen, L.F.; Caplin, A.D. Vortex dynamics in superconducting MgB_2 and prospects for applications. *Nature* **2001**, *410*, 563–565. [CrossRef]
5. Larbalestier, D.; Gurevich, A.; Feldmann, D.M.; Polyanskii, A. High-T_c superconducting materials for electric power applications. *Nature* **2001**, *414*, 368–377. [CrossRef]
6. Naito, M.; Ueda, K. MgB_2 thin films for superconducting electronics. *Supercond. Sci. Technol.* **2004**, *17*, R1–R18. [CrossRef]
7. Ueda, S.; Naito, M. As-grown superconducting MgB_2 thin films prepared by molecular beam epitaxy. *Appl. Phys. Lett.* **2001**, *79*, 2046. [CrossRef]
8. Kang, W.N.; Kim, H.-J.; Choi, E.-M.; Jung, C.U.; Lee, S.-I. MgB_2 superconducting thin films with a transition temperature of 39 kelvin. *Science* **2001**, *292*, 1521–1523. [CrossRef] [PubMed]
9. Eom, C.B.; Lee, M.K.; Choi, J.H.; Belenky, L.J.; Song, X.; Cooley, L.D.; Naus, M.T.; Patnaik, S.; Jiang, J.; Rikel, M.; et al. High critical current density and enhanced irreversibility field in superconducting MgB_2 thin films. *Nature* **2001**, *411*, 558–560. [CrossRef]
10. Christen, H.M.; Zhai, H.Y.; Cantoni, C.; Paranthaman, M.; Sales, B.C.; Rouleau, C.; Norton, D.P.; Christen, D.K.; Lowndes, D.H. Superconducting magnesium diboride films with $T_c \approx 24$ K grown by pulsed laser deposition with in situ anneal. *Phys. C* **2001**, *353*, 157–161. [CrossRef]
11. Blank, D.H.A.; Hilgenkamp, H.; Brinkman, A.; Mijatovic, D.; Rijnders, G.; Rogalla, H. Superconducting MgB_2 films by pulsed-laser deposition in an in situ two-step process using multicomponent targets. *Appl. Phys. Lett.* **2001**, *79*, 394. [CrossRef]
12. Komori, K.; Kawagishi, K.; Takano, Y.; Fujii, H.; Arisawa, S.; Kumakura, H.; Fukutomi, M. Approach for the fabrication of MgB_2 superconducting tape with large in-field transport critical current density. *Appl. Phys. Lett.* **2002**, *81*, 1047. [CrossRef]
13. Zhao, Y.; Ionescu, M.; Pan, A.V.; Dou, S.X.; Collings, E.W. In situ annealing of superconducting MgB_2 films prepared by pulsed laser deposition. *Supercond. Sci. Technol.* **2003**, *16*, 1487–1492. [CrossRef]
14. Badica, P.; Togano, K.; Awaji, S.; Watanabe, K. Growth of superconducting MgB_2 films by pulsed-laser deposition using a Nd–YAG laser. *Supercond. Sci. Technol.* **2006**, *19*, 242–246. [CrossRef]
15. Matsumoto, A.; Kobayashi, Y.; Takahashi, K.; Kumakura, H.; Kitaguchi, H. MgB_2 thin films fabricated by a precursor and post-annealing method have a high Jc in high magnetic fields. *Appl. Phys. Express* **2008**, *1*, 021702. [CrossRef]
16. Kitaguchi, H.; Matsumoto, A.; Kumakura, H.; Doi, T.; Yamamoto, H.; Saitoh, K.; Sosiati, H.; Hata, S. MgB_2 films with very high critical current densities due to strong grain boundary pinning. *Appl. Phys. Lett.* **2004**, *85*, 2842. [CrossRef]
17. Horii, S.; Ichinose, A.; Iwanaka, T.; Kusunoki, T.; Doi, T. High infield performance and critical temperatures in post-annealed MgB_2 films. *Appl. Phys. Express* **2018**, *11*, 093102. [CrossRef]
18. Kambe, H.; Kawayama, I.; Kitamura, N.; Ichinose, A.; Iwanaka, T.; Kusunoki, T.; Doi, T. Increase in the infield critical current density of MgB_2 thin films by high-temperature post-annealing. *Appl. Phys. Express* **2021**, *14*, 025504. [CrossRef]
19. Zeng, X.; Pogrebnyakov, A.V.; Kotcharov, A.; Jones, J.E.; Xi, X.X.; Lysczek, E.M.; Redwing, J.M.; Xu, S.; Li, Q.; Lettieri, J.; et al. In situ epitaxial MgB_2 thin films for superconducting electronics. *Nat. Mater.* **2002**, *1*, 35–38. [CrossRef] [PubMed]
20. Pogrebnyakov, A.V.; Redwing, J.M.; Jones, J.E.; Xi, X.X.; Xu, S.Y.; Qi, L.; Vaithyanathan, V.; Schlom, D.G. Thickness dependence of the properties of epitaxial thin films grown by hybrid physical-chemical vapor deposition. *Appl. Phys. Lett.* **2003**, *82*, 4319. [CrossRef]
21. Zhuang, C.G.; Meng, S.; Zhang, C.Y.; Feng, Q.R.; Gan, Z.Z.; Yang, H.; Jia, Y.; Wen, H.H.; Xi, X.X. Ultrahigh current-carrying capability in clean MgB_2 films. *J. Appl. Phys.* **2008**, *104*, 013924. [CrossRef]
22. Moeckly, B.H.; Ruby, W.S. Growth of high-quality large-area MgB_2 thin films by reactive evaporation. *Supercond. Sci. Technol.* **2006**, *19*, L21–L24. [CrossRef]

23. Ahn, J.-R.; Lee, S.-G.; Hwang, Y.; Sung, G.Y.; Kim, D.K. Fabrication of MgB_2 thin film by rf magnetron sputtering. *Phys. C* **2003**, *388–389*, 127–128. [CrossRef]
24. Yamamoto, A.; Shimoyama, J.; Ueda, S.; Katsura, Y.; Horii, S.; Kishio, K. Synthesis of high J_c MgB_2 bulks with high reproducibility by a modified powder-in-tube method. *Supercond. Sci. Technol.* **2004**, *17*, 921–925. [CrossRef]
25. Yamamoto, A.; Ishihara, A.; Tomita, M.; Kishio, K. Permanent magnet with MgB_2 bulk superconductor. *Appl. Phys. Lett.* **2014**, *105*, 032601. [CrossRef]
26. Sugino, S.; Yamamoto, A.; Shimoyama, J.; Kishio, K. Enhanced trapped field in MgB_2 bulk magnets by tuning grain boundary pinning through milling. *Supercond. Sci. Technol.* **2015**, *28*, 055016. [CrossRef]
27. Jung, C.U.; Kim, H.-J.; Park, M.-S.; Kim, M.-S.; Kim, J.Y.; Du, Z.; Lee, S.-I.; Kim, K.H.; Betts, J.B.; Jaime, M.; et al. Effects of unreacted Mg impurities on the transport properties of MgB_2. *Phys. C* **2002**, *377*, 21–25. [CrossRef]
28. Berenov, A.; Lockman, Z.; Qi, X.; MacManus-Driscoll, J.L.; Bugoslavsky, Y.; Cohen, L.F.; Jo, M.-H.; Stelmashenko, N.A.; Tsaneva, V.N.; Kambara, M.; et al. Growth of strongly biaxially aligned MgB_2 thin films on sapphire by postannealing of amorphous precursors. *Appl. Phys. Lett.* **2001**, *79*, 4001. [CrossRef]
29. Bean, C.P. Magnetization of Hard Superconductors. *Phys. Rev. Lett.* **1962**, *8*, 250. [CrossRef]
30. Bean, C.P. Magnetization of High-Field Superconductors. *Rev. Mod. Phys.* **1964**, *36*, 31. [CrossRef]
31. Doua, S.X.; Wanga, X.L.; Horvat, J.; Milliken, D.; Li, A.H.; Konstantinov, K.; Collings, E.W.; Sumption, M.D.; Liu, H.K. Flux jumping and a bulk-to-granular transition in the magnetization of a compacted and sintered MgB_2 superconductor. *Phys. C* **2001**, *361*, 79–83. [CrossRef]
32. Johansen, T.H.; Baziljevich, M.; Shantsev, D.V.; Goa, P.E.; Galperin, Y.M.; Kang, W.N.; Kim, H.J.; Choi, E.M.; Kim, M.-S.; Lee, S.I. Dendritic flux patterns in MgB_2 films. *Supercond. Sci. Technol.* **2001**, *14*, 726–728. [CrossRef]
33. Kovác, P.; Hušek, I.; Pérez, N.; Rosová, A.; Berek, D.; Gelušiaková, B.; Kopera, L.; Melišek, T.; Nielsch, K. Structure and properties of barrier-free MgB_2 composite wires made by internal magnesium diffusion process. *J. Alloys Compd.* **2020**, *829*, 154543. [CrossRef]
34. Kitaguchi, H.; Doi, T.; Kobayashi, Y.; Matsumoto, A.; Sosiati, H.; Hata, S.; Fukutomi, M.; Kumakura, H. Properties of MgB_2 films with very high transport critical current densities. *IEEE Trans. Appl. Supercond.* **2005**, *15*, 3313–3316. [CrossRef]